Spectral analysis of polymer microring lasers

R. C. Polson,[a] G. Levina, and Z. V. Vardeny
Department of Physics, University of Utah, Salt Lake City, Utah 84112

(Received 13 March 2000; accepted for publication 8 May 2000)

The emission spectra of microring lasers made of π-conjugated polymer films that coat glass optical fibers are analyzed with the help of a Fourier transform. This method allows for the assignment of photopumped emission lines to integral Bessel functions and a more precise determination of the laser threshold excitation intensity based on harmonic analysis. © *2000 American Institute of Physics.* [S0003-6951(00)04026-2]

A microring laser cavity offers a low loss resonance structure that has been utilized to demonstrate lasing with organic gain media[1] as well as π-conjugated polymers.[2–4] The optically pumped polymer based devices show lasing at relatively low excitation intensity threshold and are usually a demonstration of the superior polymer optical properties that allow high optical gain. Here we present a method that explains the emission lines seen in polymer microring laser spectra by using a Fourier transform of these spectra.

The Fourier transform of the laser emission spectrum can be used to determine the following: first, positive harmonics in the transform gives the product of the effective index of refraction, n, and laser cavity diameter, D. With this obtained product in hand, each emission line in the spectrum can be thereby assigned to an integer Bessel function. Second, by using the ratio of the amplitude of successive harmonics in the Fourier transform, the laser excitation intensity threshold can be more precisely determined than by a simple kink in the laser intensity output.

The polymer microring laser devices studied here were made from poly(dioctyloxy) phenylene vinylene (DOOPPV) which was synthesized by modifying a published procedure.[5] A thin polymer film was self-assembled to coat glass fibers with diameter of 125 μm.[2] These devices were pumped with the second harmonic of a Nd:yttrium–aluminum–garnet(YAG) laser at 532 nm with pulses lasting 100 ps at 100 Hz repetition rate. The measurements were done in a dynamic rough vacuum of 2 Torr. The pump beam was focused through a cylindrical lens exciting a narrow stripe on the coated fiber. The emission light was collected through a second fiber (1 mm in diameter) approximately 3 cm from the microring laser and sent to a Spex 1200 triple spectrometer, where a charged coupled device (CCD) camera recorded the light intensity. The overall spectral resolution was 0.05 nm.

Figure 1 is a typical emission spectrum of a polymer microring laser. It consists of a number of relatively sharp lines that we wish to analyze here. The equations used to describe Fabry–Perot cavities[6] work equally well here, with the substitution of the linear cavity length L by $\pi D/2$. Thus, the expected mode spacing, $\Delta\lambda$, is given by

$$\Delta\lambda = \frac{\lambda^2}{2nL} = \frac{\lambda^2}{\pi nD}. \tag{1}$$

The spacing $\Delta\lambda$ of the emission lines in Fig. 1 ranges from 0.65 to 0.70 nm. Using the strongest emission line at 629.50 nm and a diameter, D of 125 μm we get from Eq. (1) an effective refractive index, n, 1.58 that is an intermediate value between that of the glass core, $n=1.5$, and the polymer, $n=1.8$. The spacing $\Delta\lambda$ is adequately explained, but the origin of the emission lines remains undetermined.

The Fourier transform of the emission spectrum gives a more accurate value of nD, which then may be used to explain the emission lines more precisely. The expected inten-

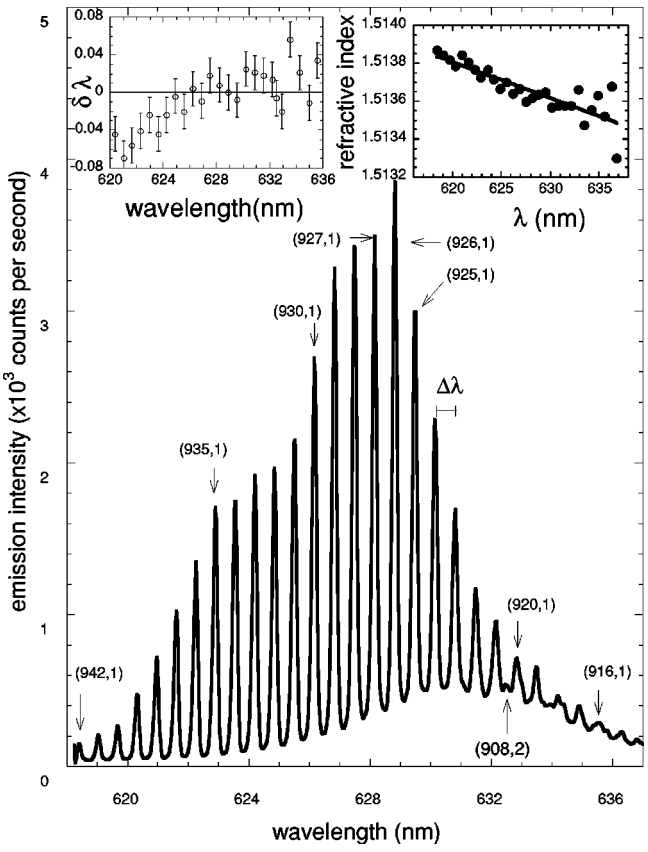

FIG. 1. Typical emission spectrum of a polymer microring laser based on DOOPPV; the line separation, $\Delta\lambda$, is assigned. The laser lines label (s,t) indicates the t zero of Bessel function s. The left inset shows the difference, $\delta\lambda$ between observed and calculated line wavelengths. The right inset shows the index of refraction versus wavelength assuming a diameter of 125 μm.

[a]Electronic mail: rpolson@mail.physics.utah.edu

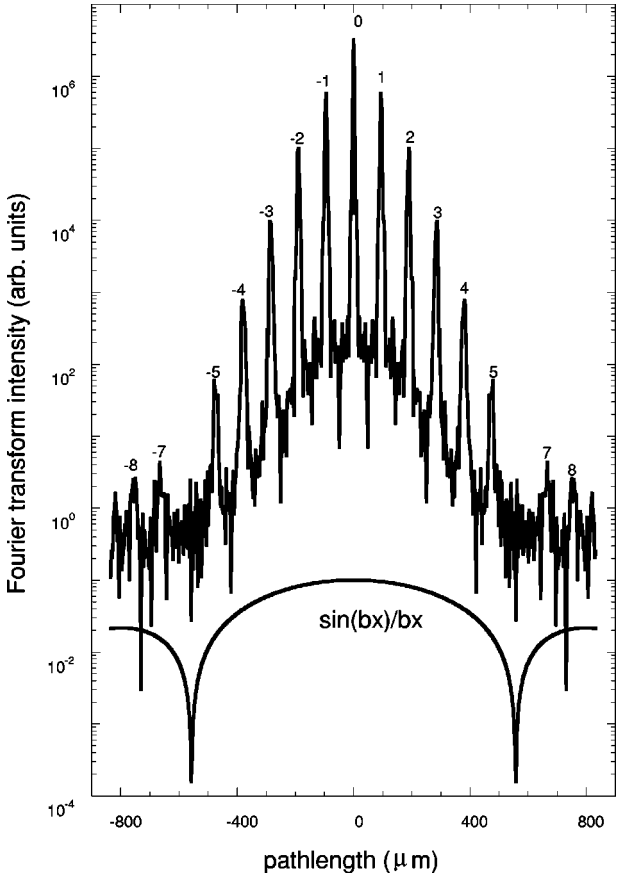

FIG. 2. Fourier transform of the spectrum given in Fig. 1. Note the apparent disappearance of the sixth harmonic. Shown at the lower part is abs[sinc(bx)] with $b=\pi/365$.

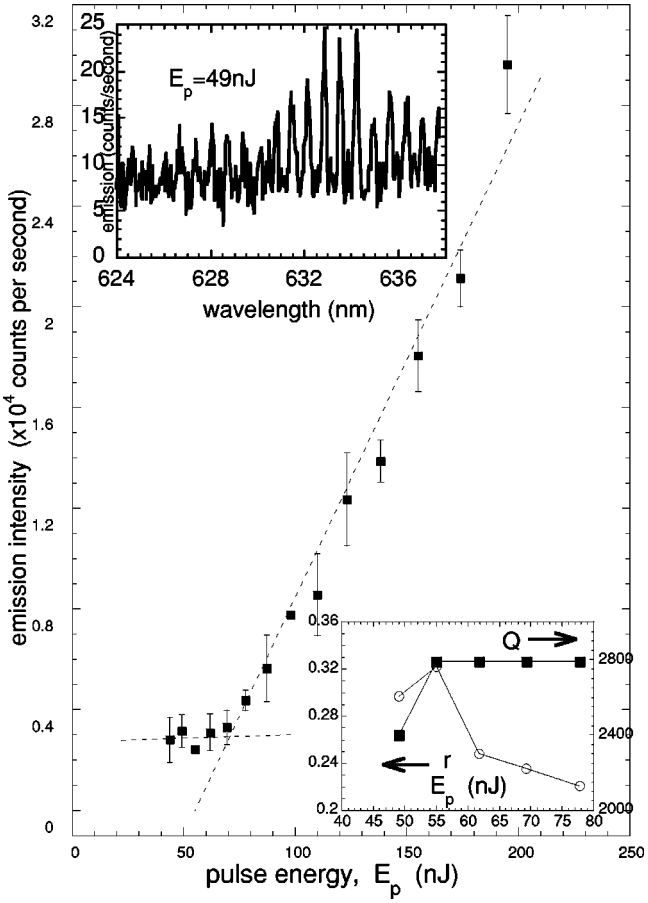

FIG. 3. Integrated emission intensity versus pulse energy, E_p. The top inset shows a spectrum at $E_p=49$ nJ. The bottom inset shows r and Q values versus pulse energy, E_p.

sity of the Fourier transform of a Fabry–Perot cavity was derived in Ref. 7. It consists of a series of equally spaced diminishing lines given by

$$I(d)=|1-R\exp(2i\Phi)|^2 \times\sum_{m=0}^{\infty}\sum_{l=0}^{\infty}\frac{R^{l+m}\exp[-2i\Phi(l-m)]}{kL(l+m+1)+i[\pi d+nL(l-m)]}. \quad (2)$$

Here k is the wavevector, $k=2\pi/\lambda$, d is the conjugate variable to wavevector, l,m are integers, Φ is the phase change upon reflection at the mirrors, and R is the mirror reflectivity. The important part of this expression is that peaks are produced whenever the imaginary part of the denominator goes to zero. This occurs when d is a multiple of nL/π, or $nD/2$ with the circular geometry used here.

Figure 2 is the Fourier transform of the emission spectrum, that was shown in Fig. 1, plotted on a log scale. If the emission spectrum is measured in wavevector space with the unconventional units $\mu\mathrm{m}^{-1}$, or $10\,000\,\mathrm{cm}^{-1}$, then the transform units are in μm, that are convenient for obtaining an effective index of refraction.

Transform harmonics peaks are at multiples of $nD/2$, which in the case of Fig. 2 occur at 94.595 μm. Also in the Fourier transform of Fig. 2 an envelope described by $\sin(bx)/bx$ is present because of a limited collection angle of our experimental setup.[8] This manifests itself most clearly with the apparent disappearance of the sixth harmonic peak. Shown schematically in Fig. 2 in the lower part is the function abs[sinc(bx)], with b corresponding to $\pi/385$. Actually b is the angle in real space which is covered by our detection system; working with the geometry of a 1-mm-diam collection fiber, this indicates that the distance of the collection fiber to the ring laser was about 30 mm.

The accuracy of nD and the high cavity quality factor, Q, used together offer a complete explanation of the laser emission spectrum. The simplification used here is that at the boundary of the polymer air interface the radial function describing the field is zero. In a simple circular geometry the radial function is described by a Bessel function[9] $J_s(2\pi n\rho/\lambda)$, where $\rho=D/2$. This function goes to zero whenever the argument is equal to a zero of the Bessel function, i.e., $2\pi n\rho/\lambda=X_{st}$, where X_{st} is the t zero of Bessel function of integer s.

In Fig. 1 the peak with the highest intensity is at 629.50 nm. Mode assignment comes from determining the order of the Bessel function. Since Bessel function of order s has s modes around the circumference, the starting s is $\pi nD/\lambda$. Using the value of nD from the Fourier transform, we get s as 944. The geometry of the devices, a thin layer of active material on a much larger core, suggests using the first or possibly second zero of the Bessel function. The first zero of Bessel function 944 obtained from a numeric table or from commercially available mathematics software has a value of 962.31. Based on X_{st} above, this gives an expected wavelength of 617.65 nm, that is incorrect. By inspecting s values near 944 we discovered a value of s that works better, namely $s=926$. This gives a predicted wavelength value of

TABLE I. Comparison of Q and r values for the six lowest excitation energies shown in Fig. 3.

Intensity (nJ/pulse)	44	49	55	61	69	78
Q direct	no harmonics	2400	2790	2790	2790	2790
r	n/a	0.297	0.322	0.248	0.237	0.221

629.49 nm. The neighboring peak on the left, at 628.85 nm matches with Bessel function 927, the predicted value is 628.82 nm. The neighboring peak on the right at 630.15 nm gives Bessel function 925 with predicted value 630.16 nm. The entire spectra corresponds to successive values of s starting with 942 for the most blue peak at 618.40 nm and continuing to the most red peak at 633.40 nm and s value 916. There are no adjustable parameters, only the determination of the correct order, s. The weak line at 632.5 nm is noteworthy because it is the only line to come from a second zero, namely the second zero of the Bessel function 908. The left insert of Fig. 1 shows the difference, $\delta\lambda$ between the wavelengths of predicted and experimental peaks. Based on the apparent agreement between experiment and model calculation, we conclude that the entire spectrum is well explained with the product nD and a series of integers for s.

The apparent systematic error in Fig. 1 left inset could possibly be from a calibration error. A neon plasma tube was used as a reference and four well spaced lines were used to calibrate the emission spectrum. The calibration is completely linear over the range observed. We therefore conclude that there is something real behind the systematic error occurrence of Fig. 1 left inset. Solving for n, $n = X_{st}\lambda_{obs}/\pi D$, and assuming a constant value for D at 125 μm, we get $n(\lambda)$ as seen in the right insert of Fig. 1. The points fall on the line $n = 1.5256 - 1.895 \times 10^{-5}\lambda$, which describes the change of refractive index with wavelength.

Another property of a Fabry–Perot cavity is the resolving power. The resolving power of an interferometer, or Q of a resonator is the following:[10]

$$Q = \frac{2\pi nL}{\lambda}\frac{\sqrt{r}}{1-r}, \tag{3}$$

where r is $R\exp[-(\alpha-\gamma)L]$, R is the mirror reflectivity α and γ are the optical loss and gain per length, respectively. When $r>1$, then Eq. (3) is no longer valid, since gain exceeds loss; this is the important criterion for determining lasing threshold.

In simple cases of small absorption, narrow wavelength window, and when the device is below threshold,[7,11] the ratio of one harmonic peak's amplitude to the next is given by r. The Q of the cavity can be also estimated directly from the emission spectra by measuring the width of emission modes, $Q = \lambda/d\lambda$ where $d\lambda$ is the full width at half maximum. Threshold analysis is simply plotting the Q and r values versus the excitation intensity. When lasing threshold is crossed, there will be an abrupt change in both Q and r.

Figure 3 shows the emission intensity versus excitation energy per pulse, E_p of a different device than the one shown in Fig. 1. With the exception of the lowest E_p of 44 nJ, all the emission spectra show narrow lines. *The appearance of these narrow lines do not indicate lasing*. Figure 3 shows the typical kink in emission intensity versus E_p that indicates the presence of lasing. However, the exact threshold location is difficult to determine by the figure. Using the straight line model, the intersection of the two lines is at $E_p = 69$ nJ and the line crosses zero at $E_p = 55$ nJ. The determination of lasing threshold would be somewhat arbitrary. Table I shows the Q and r values for the lowest five excitation energies. From the lower inset of Fig. 3 at 61 nJ/pulse there is a large change in Q and r; we conjecture that the device is lasing at this pump energy. The top insert of Fig. 3 is the spectrum at $E_p = 49$ nJ/pulse, which is below threshold. We note that the narrow emission lines present in this spectrum do not by themselves indicate lasing.

In conclusion, the exact determination of Bessel functions for a microring polymer laser is accomplished with information provided from the Fourier transform. Also with the aid of the Fourier transform, a method is developed in which the laser threshold is determined by the ratio of transformed harmonics. The lasing threshold can be thus experimentally determined without knowing the reflectivity or the exact gain dependence on pumping.

The authors wish to thank A. Chipouline and M. Shkunkov for technical assistance. This work was supported in part by NSF Grant No. DMR 9732820.

[1] M. Kuwata-Gonokami, R. H. Jordan, A. Dodabalapur, H. E. Katz, M. L. Schilling, and R. E. Slusher, Opt. Lett. **20**, 2093 (1995).
[2] S. V. Frolov, M. Shkunov, Z. V. Vardeny, and K. Yoshino, Phys. Rev. B **56**, R4363 (1997).
[3] Y. Kawabe, Ch. Spiegelberg, A. Sch-lzgen, M. F. Nabor, B. Kippelen, E. A. Mash, P. M. Allemand, M. Kuwata-Gonokami, K. Takeda, and N. Peyghambarian, Appl. Phys. Lett. **72**, 141 (1998).
[4] S. V. Frolov, Z. V. Vardeny, and K. Yoshino, Appl. Phys. Lett. **72**, 1802 (1998).
[5] N. N. Barashkov, D. J. Guerrero, H. J. Olivos, and J. P. Ferraris, Synth. Met. **75**, 153 (1995).
[6] H. P. Weber and R. Ulrich, Appl. Phys. Lett. **19**, 38 (1971).
[7] D. Hofsttetter and R. L. Thornton, Appl. Phys. Lett. **72**, 404 (1998).
[8] V. G. Cooper, Appl. Opt. **10**, 525 (1971).
[9] J. D. Jackson, *Classical Electrodynamics*, 2nd ed. (Wiley, New York, 1975).
[10] N. V. Karlov, *Lectures on Quantum Mechanics* (Chemical Rubber, Boca Raton, 1993).
[11] D. Hofsttetter and R. L. Thornton, Opt. Lett. **32**, 1831 (1997).